Chapter 5

Reversible Multifunction Multimode On-board Power Processor with Inherent V2G Operation

5.1 Introduction

This chapter presents a reversible multifunction multimode On-board power processor with inherent V2G operation. The on-board power processor provides grid-to-vehicle (G2V) charging, vehicle-to-grid (V2G) power supply, vehicle-to-vehicle (V2V) charging, and motoring mode (MM) operation. In addition to these operations, the proposed power processor also gives two regulated DC outputs, i.e., 12 V and 72 V simultaneously, in all the operating modes. These regulated DC outputs help to provide a power supply to the auxiliaries of the EV cabin. The 12 V DC output of the proposed processor eliminates the need for an additional 12 V battery to supply the EV cabin's low-power auxiliaries. Further, the 72 V regulated output reduces the current requirement to feed the high-power auxiliaries. During G2V low-power, the proposed power processor maintains the unity power factor on the grid side, and because of its bidirectional capability, it also facilitates V2G operation. Moreover, the same power processor is capable of restructuring itself for motor drive and V2V charging. In V2V charging, the proposed power processor can act as the transmitter and receiver in connected vehicles for energy exchange. Conventionally, different converters are required for these functions, as shown in Fig.5. 1.

Researchers integrate one or more functions into a single converter to reduce the cost of EVs [124]. There are possible ways to integrate the on-board power converter with different functionalities that are given in Fig.5. 2.

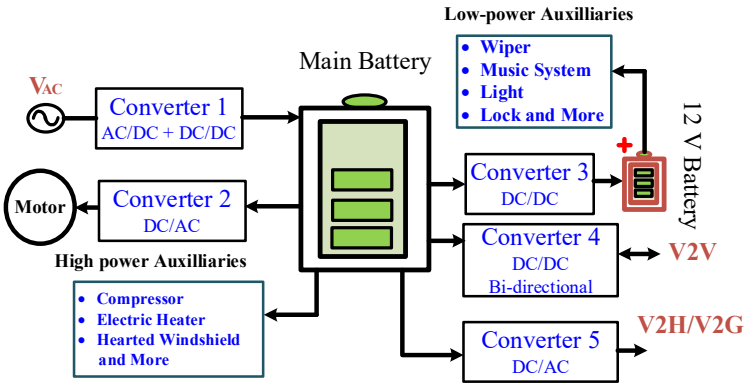

Fig.5. 1 Purpose of different converters and their operation in a conventional system.

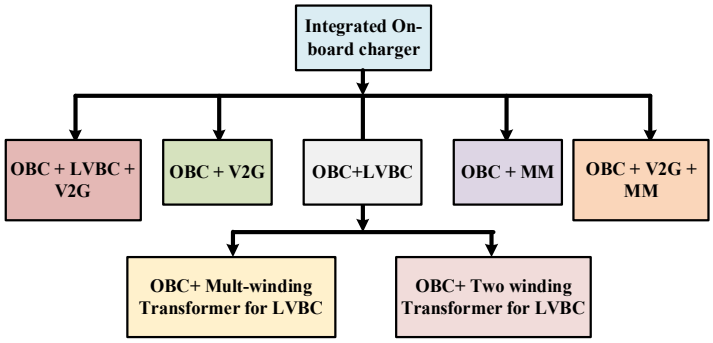

Fig.5. 2 Integrated on-board chargers with different functionalities.

The contributions of the proposed converter are as follows:

1) The proposed power processor performs G2V, V2G, V2V, and motoring operations while generating multiple outputs. It is programmed with three additional switches to facilitate all four functions.
2) During all four functions, it generates two regulated DC outputs: 1) 12V and 2) 72V for auxiliaries of the EV cabin.
3) The 12V powers low-power auxiliaries, eliminating the requirement of an additional 12V battery and its charger.
4) The 72 V boost output voltage in a 48 V low-power EV battery reduces the current requirement for the high-power auxiliaries.
5) The proposed power processor reduces the switch count and the overall cost.

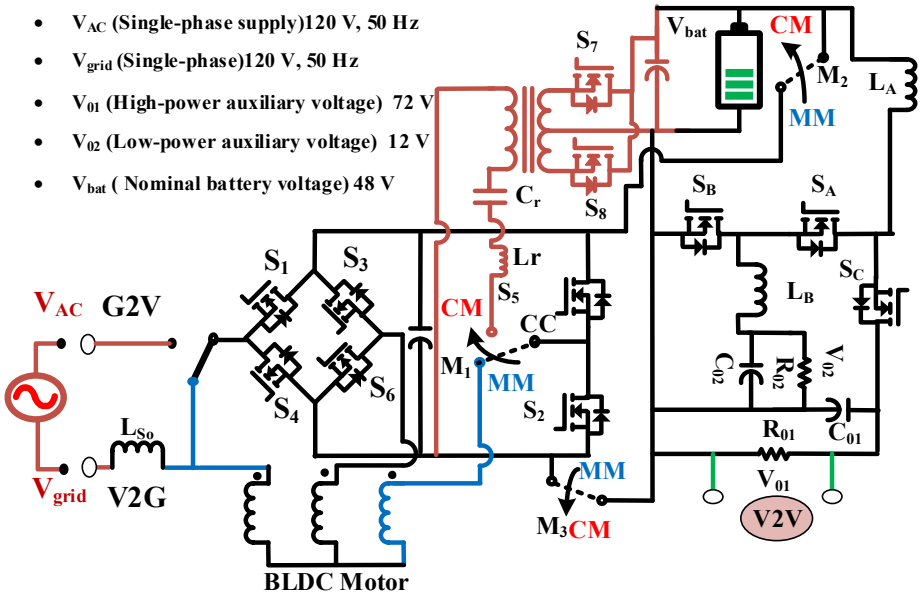

Fig.5. 3 Circuit diagram of the proposed power converter.

The proposed power processor is evaluated for low-power EVs that operate with a main battery voltage of 48 V. Some examples of low-power EVs include the Arcimoto FUV, GEM e4, Mahindra e20, etc. The proposed converter can be adapted for higher-power EVs by enhancing its power-handling capabilities.

5.2 Operation of the proposed integrated power converter in its different functions

The idea of the proposed converter is to provide grid-to-vehicle (G2V), vehicle-to-grid (V2G), vehicle-to-vehicle (V2V), and motoring mode operations (MM), with the auxiliary power supply to the EV cabin, as shown in Fig.5. 3. This integrated converter uses a lower number of switches than existing power converters with similar prior works and provides more functionalities.

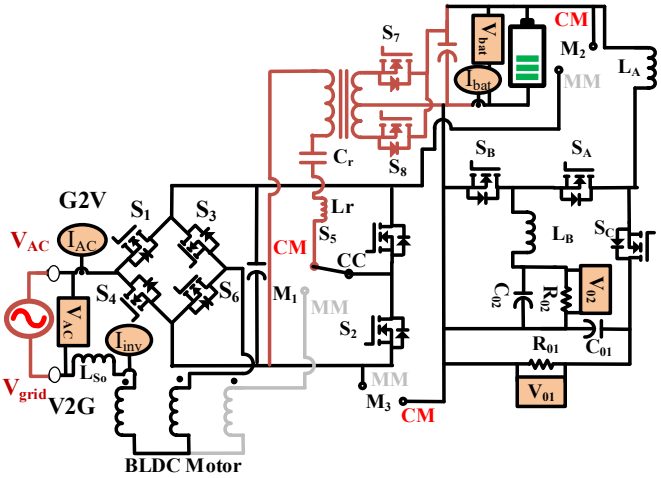

Fig.5. 4 Circuit diagram of the proposed converter in single-phase charging and vehicle-to-grid power supply.

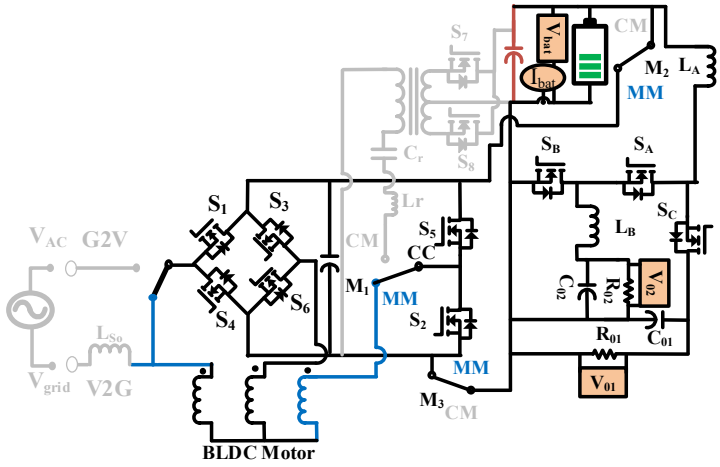

Fig.5. 5 Circuit diagram of the proposed converter in motoring mode.

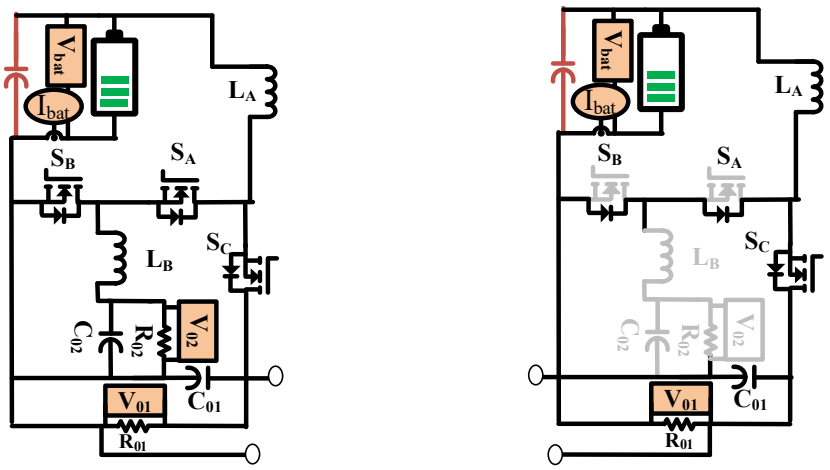

(a) (b)

Fig.5. 6 The connection of the circuit diagram from both vehicles during V2V charging, (a) circuit of energy supplier, and (b) circuit of energy acceptor.

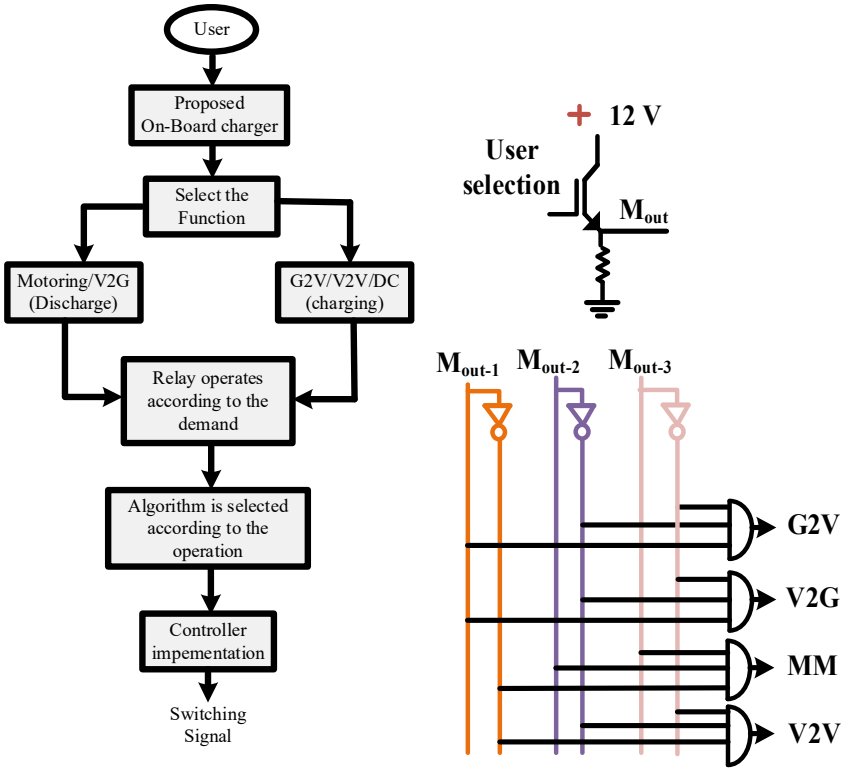

(a) (b)

Fig.5. 7 Flowchart for implementation of on-board charger in respective mode, and (b) user selection of their respective mode.

The individual operating modes of the proposed converter are illustrated in Fig.5. 4, Fig.5. 5, and Fig.5. 6. The implementation of these operations is depicted in the flowchart provided in Fig.5. 7(a). Transitioning from one mode to another is facilitated by three additional switches, which are controlled by the switching logic shown in Fig.5. 7(b). Each additional

switch is configured to implement the selected function based on the desired operation. This section explains each mode transformation of the proposed circuit individually.

5.2.1 Charging Mode operation of the proposed power processor

The configuration of the proposed converter for G2V charging is illustrated in Fig.5. 4. The charging mode is activated by connecting the charging connector to the input port. Switch M_1 connects to the common connection (CC) along with the charging mode connection (CM), while switches M_2 and M_3 remain open. It charges the battery using a single-phase AC supply and maintains a unity power factor (UPF) at the source terminal. While charging, the proposed converter generates two additional outputs in addition to charging the high-voltage battery (HVB). One of these outputs supports the cabin's low-power auxiliaries, while the other supports the high-power auxiliaries. To maintain the unity power factor (UPF), the load on the source inductor has been reduced by incorporating the motor's field winding. The phase A and phase B windings of the BLDC motor are connected to the source inductor. During the charging operation, the motor does not move. This can be observed in the simulation results of the motor's field winding current and its resulting flux during the charging operation in Fig.5. 8. Therefore, a complete cycle cannot produce any revolving field to drive the motor.

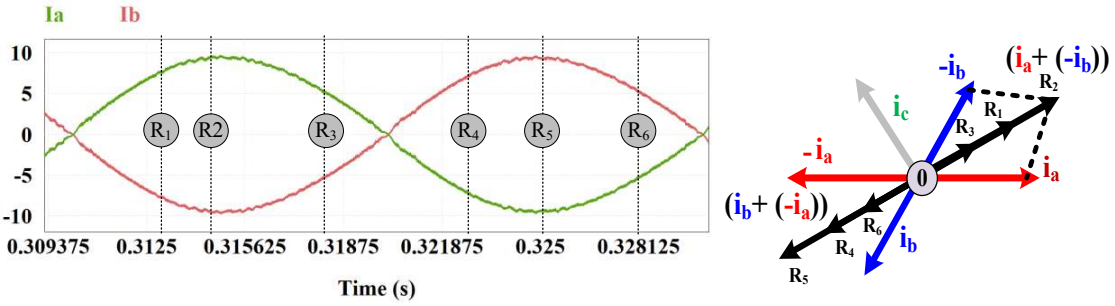

(a) (b)

Fig.5. 8 (a) Simulation result of the current of BLDC field winding during single-phase charging, and (b) phase diagram of the current in phases (a) and (b).

5.2.2 Motoring mode operation of the proposed power processor

The charging plug is removed from the socket to switch from charging to motoring mode. Additionally, switch M_1's common connection (CC) connects to the motoring mode connector (MM), while switches M_2 and M_3 also connect their CC to the MM connector, as shown in Fig.5. 5. During the motoring operation, power is drawn from the battery to drive the motor, and auxiliary voltages are generated to provide power support for the cabin. The hall sensor

detects the rotor's position to operate the motor. The converter is then adjusted based on the rotor's position.

5.2.3 V2G connection from the proposed converter

The bi-directional property of the proposed converter supports the V2G operation, and the circuit diagram remains the same as for the G2V operation, as shown in Fig.5. 4. To transfer power from the battery to the grid, switches S_7 and S_8 are activated, charging the DC-link voltage with the assistance of a step-up transformer. The transformer is used as a resonant tank during the charging process. Furthermore, switches S_1, S_3, S_4, and S_6 are activated according to the control algorithm to maintain the rated voltage or current based on home or grid demand.

5.2.4 V2V charging from the proposed converter

V2V charging is achieved by directly connecting the proposed power converter from both vehicles. The circuit diagram for V2V energy transfer is illustrated in Fig.5. 6. In the circuit diagram, energy flows from left to right. The left section of the circuit diagram illustrates the energy supply circuit of the proposed power processor. The right section of the circuit diagram illustrates the energy acceptance circuit of the proposed power processor. During operation, the other components of the proposed converter remain inactive.

Table 5. 1 Specification of the power level in their respective mode of operation

Mode of operation	**Power IN**	**Voltage and Current rating at the load**			**Output Power (Watts)**
Charging	V_{in}= 120 V, I_{in} = 6.5 A	V_{bat}= 48V, I_{bat} = 5.5 A	V_{01}=72 V, I_{01} =5.5 A	V_{02}=12 V, I_{02} = 5A	264+396+60 = 720
Motoring	V_{bat} = 48 V I_{bat} = 21 A	V_{BLDC}=48 V, I_{BLDC} = 10 A	V_{01}=72 V, I_{01} =5.5 A	V_{02}= 12 V, I_{02} = 5 A	480+396+60 =936
V2V	V_{bat} = 48 V I_{bat} = 10 A	---	V_{01}=72 V, I_{01} =5.5 A	V_{02}= 12 V, I_{02} = 5 A	396+60= 456
V2G	V_{bat} = 48 V I_{bat} = 22A	V_{AC}=120 V Iac = 4.2 A	V_{01}=72 V, I_{01} =5.5 A	V_{02}= 12 V, I_{02} = 5 A	480+396+60=960
V_{bat} and I_{bat} (battery voltage and current), V_{01} and I_{01} (High-power auxiliaries' voltage and current), V_{02} and I_{02} (Low-Power auxiliaries' voltage and current), V_{BLDC} and I_{BLDC} (motor voltage and current rating), Vac= grid voltage, Iac= injected grid current					

5.3 Control Logic of the Proposed power processor

The controller of the proposed power processor is designed to operate its respective functions within the rated value in its respective modes of operation. The operating range of the proposed converter is shown in Table 5. 1. The control technique of the individual mode is given in Fig.5. 9.

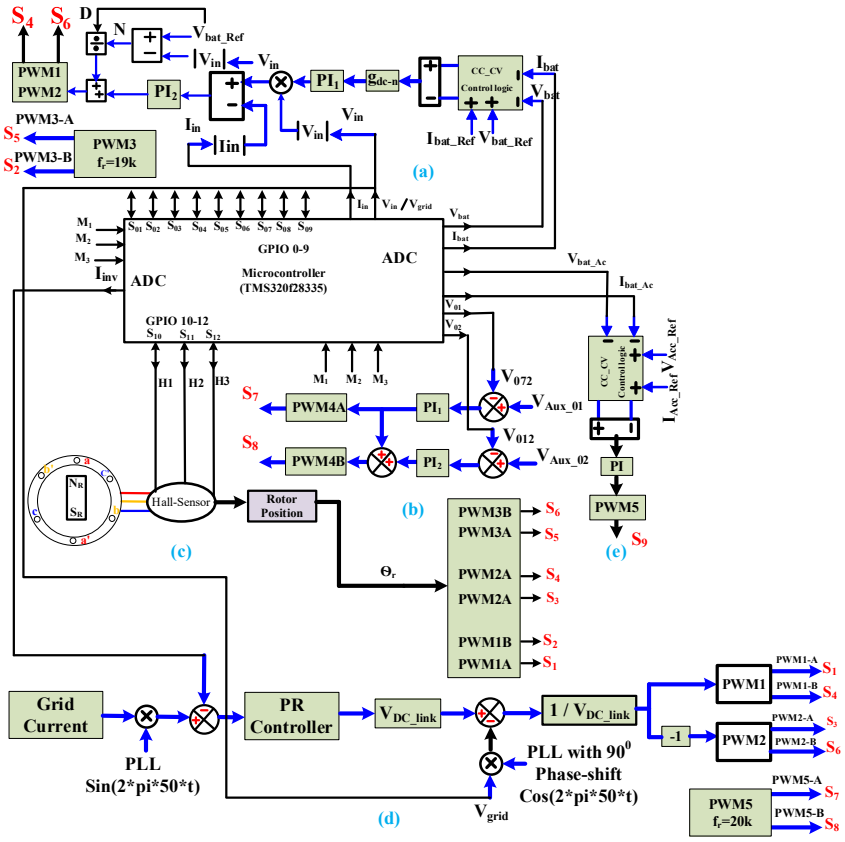

Fig.5. 9 control logic of the proposed power processor, (a) control logic for unity power factor with CC-CV charging, (b) control logic for auxiliary power supply, (c) control logic for motor drive, (d) control logic for V2G power supply, and (e) control logic for energy acceptor vehicle.

5.3.1 Control process of G2V charging

Six parameters are monitored to implement the G2V operation: 1) input source voltage (V_{AC}), 2) input source current (I_{AC}), 3) battery voltage (V_{bat}), 4) battery current (I_{bat}), and 5) and 6) for the low and high-power auxiliaries' voltages (V_{02} and V_{01}), as shown in Fig.5. 9(a). During G2V charging, the proposed converter maintains a unity power factor at the source terminal while charging the battery using constant-current and constant-voltage (CC-CV) techniques[125]. The state of charge (SOC) is used as the reference for transitioning from constant current (CC) to constant voltage (CV), typically around 70% of the SOC [126] [127][128]. The error from the CC-CV condition is processed by the PI_1 controller, which helps maintain the voltage and current at selected values. The controller's bandwidth is kept low to avoid doubling the line frequency [129]. Its output is multiplied by the rectified value of the V_{AC} and then subtracted from the I_{AC} to achieve zero crossing. The error is minimised by the PI_2 controller, which has a bandwidth of one-tenth of the switching frequency. The generated pulse is simultaneously sent to switches S_4 and S_6.

5.3.2 Auxiliary power supply of the proposed converter

The auxiliary power supply of the proposed converter meets the power demands of both low and high-power auxiliaries in EVs. The state space transfer function, representing the small signal analysis of the auxiliary power supply, is given in Eq. 1. These auxiliary power supplies are available in each mode of operation, removing the need for an additional 12 V battery and its charger. The control technique for the multioutput is given in Fig.5. 9(b). It regulates both the 12 V and 72 V from a 48 V battery. The desired boost output voltage is subtracted from the measured 72 V (V_{01}), and the resulting error is processed by the PI_1 controller. The V_{01}/D_1 transfer function is used to design the PI_1 controller with D_2 set to zero. In this context, D_1 represents the complete shoot-through interval (when S_A and S_B are ON), while D_2 corresponds to the power interval (when S_A is ON and S_B is OFF). The output activates the S_B switch. The desired buck output is subtracted from the measured 12 V (V_{02}), and the resulting error is passed through the PI_2 controller. The PI_2 controller is designed using the V_{02} / D_2 transfer function while keeping D_1 at zero. The output from the PI_2 controller is combined with that of the PI_1 controller. The sum of these outputs activates the S_A switch.

$$\begin{bmatrix} \dot{\hat{i}}_{LA} \\ \dot{\hat{i}}_{LB} \\ \dot{\hat{v}}_{C01} \\ \dot{\hat{v}}_{C02} \end{bmatrix} = \begin{bmatrix} 0 & 0 & \frac{-(1-D_1)}{L_A} & 0 \\ 0 & 0 & \frac{D_2}{L_B} & \frac{-1}{L_B} \\ \frac{(1-D_1)}{C_{01}} & \frac{-D_2}{C_{01}} & \frac{-1}{R_{01}C_{01}} & 0 \\ 0 & \frac{1}{C_{02}} & 0 & \frac{-1}{R_{02}C_{02}} \end{bmatrix} \begin{bmatrix} \hat{i}_{LA} \\ \hat{i}_{LB} \\ \hat{v}_{01} \\ \hat{v}_{02} \end{bmatrix} + \begin{bmatrix} \frac{V_{01}}{L_A} & 0 & \frac{-i_{LA}}{C_{01}} & 0 \end{bmatrix}^T d_1 + \begin{bmatrix} 0 & \frac{V_{01}}{L_B} & \frac{-i_{LB}}{C_{01}} & 0 \end{bmatrix}^T \widehat{d_2} \tag{1}$$

$$\left[\frac{\hat{V}_{bat-acct}}{\hat{D}_C}\right] = \frac{S^1}{S^2 + \frac{S^1}{R_{01}C_{01}} + \frac{1}{L_A C_{01}}} \tag{2}$$

5.3.3 V2V control operation of the proposed converter

In V2V charging, the proposed power converter from both vehicles is directly connected. During this process, only the multioutput features of the proposed converter remain active for energy transfer. In the energy supplier vehicle, the control logic is shown in Fig.5. 9(b) is activated, while the energy acceptor vehicle connects to the V_{01} output of the energy supplier vehicle. In the energy acceptor vehicle, the control logic is illustrated in Fig.5. 9(e) is activated. The PI controller parameters for the energy acceptor are adjusted using the transfer function of $V_{bat\text{-}acct}$ / D_C, as given in Eq.2. Here, D_c represents the duty ratio of switch S_C. The V2V

operation is implemented by the two-step process utilizing the six switches of the connected proposed power converters.

5.3.4 Speed control of the BLDC motor

In motoring mode, the same converter drives the BLDC motor by switching the control technique from charging to motoring. The speed of the BLDC motor is controlled either by varying the direct voltage applied to the converter or by adjusting the converter's PWM signal. The motor speed varies proportionally with the magnitude of the applied voltage: higher voltage increases the motor speed, while lower voltage decreases it.

Conversely, in the PWM scheme, the motor speed is controlled by adjusting the on and off durations of the switch. The motor's speed increases as the turn-on time of the PWM width increases, and decreases as the turn-on time of the PWM width decreases. Determining the exact position of the rotor is crucial for driving the BLDC motor. In the proposed system, three Hall effect sensors detect the rotor's position, and the converter is activated using the existing High-PWM Low-ON switching technique to drive the BLDC motor. The PWM width regulates the motor's speed[130]. The PWM switching is applied to the upper switches S_1, S_3, and S_5, while all switches, including S_4, S_6, and S_2, remain ON during their respective six-step commutation intervals. The control technique of the BLDC motor is shown in Fig.5. 9(c).

5.3.5 Control technique of the V2G operation

The rapid growth of electric vehicles (EVs) is influencing the stability of the grid. Feeding power from vehicles to the grid can help stabilize it during surges in energy demand. The control technique for the V2G is given in Fig.5. 9(d). In this control technique, the desired current value for dumping into the grid is multiplied by the PLL (Sin(2π50t)) and then processed through the proportional-resonant (PR) controller.

$$H_{AC}(s) = K_p + \frac{2K_i S}{S^2 + {w_o}^2} \tag{3}$$

$$K_p = \frac{\alpha\sqrt{\alpha}\,\omega_0 L - r}{V_{DC-link}} \tag{4}$$

$$K_i = \frac{{\omega_0}^2 L(\alpha^2 - 1)}{2V_{DC-link}} \tag{5}$$

Where: L and r represent the inductance and its internal resistance, respectively; ω_0 is the angular frequency of the power line; and $\alpha=2\zeta+1$, where ζ is the damping factor.

The equation of the PR controller is given in (3), and its K_P and K_i value is calculated by the Naslin Polynomial method[131]. Its value is given in (4) and (5) respectively. The output of the PR controller is passed through the DC-link voltage. The output from the DC-link voltage is subtracted from the grid voltage, which is synchronized with the grid phase. Further, it passes through the 1/ DC-link voltage and generates the pulse for switches S_1, S_4, S_3, and S_6.

5.4 Comparative analysis of the proposed converter

The uniqueness of the proposed converter with similar prior work can be understood through a comparative analysis, cost analysis, and component utilization factor (CUF).

5.4.1 Comparative analysis with similar prior works

Table 5. 2 Comparison with functions and switch counts in similar prior works

L.No.	Modes of operation				Multi output	Requirement of Auxiliary Battery & its charger		Function	Galvanic Isolation	Switches		Additional Switch for Mode Transfer	Total Switches
	G2V	V2G	V2V	MM		12 V	Charger			MOSFET	Diode		
[36]	✓	×	×	×	✓	✓	×	2	×	10	2	2	14
[132]	✓	✓	×	×	×	✓	✓	2	✓	8	2	0	10
[70]	✓	✓	×	×	✓	✓	×	3	✓	12	0	3	15
[72]	✓	✓	×	✓	×	✓	✓	3	✓	16	0	1	17
[133]	✓	✓	✓	✓	×	✓	✓	4	×	12	0	3	15
Proposed	✓	✓	✓	✓	✓	×	×	5	✓	11	0	3	14

The comparative analysis with similar prior work is shown in Table 5. 2 . The comparison is stabilized with multifunctional features such as G2V charging, V2G power supply, V2V charging, motoring mode (MM) operation, and the auxiliary power supply for the EV cabin. In EVs, along with the main battery, an additional 12 V battery and its charger are required for the cabin power supply. The available regulated multioutput during all modes of operation eliminates the requirement for a 12 V battery and its charger in the proposed converter. Further, galvanic isolation is required to protect the EV from the fault current at the grid side, which is available in the proposed power converter. A total of 14 switches have been used, including three additional switches for the mode transform in the proposed power processor.

5.4.2 Cost analysis with similar prior work

The comparative cost analysis between the proposed converter and similar prior work is illustrated in the bar diagram in Fig.5. 10. This analysis compares the components used in the

proposed converter with similar prior work, with maximum function, and with fewer switch counts. For clarity, the prices of these components have been used as reference points. The proposed converter utilizes 11 switches, with part number IPW60R040CFD7, and three additional switches, with part number V23076-A3001-C132. However, the conventional converter has 12 switches along with three additional switches, but it lacks the multioutput capabilities found in the proposed system [133]. The cost analysis includes the switches, gate driver (FOD3184), a heat sink (1960012091T00S), and other accessories. The proposed converter eliminates the need for an additional 12 V battery and charger, as the power demand is supplied by the main battery. The proposed converter offers a total cost savings of approximately $55 compared to the conventional system.

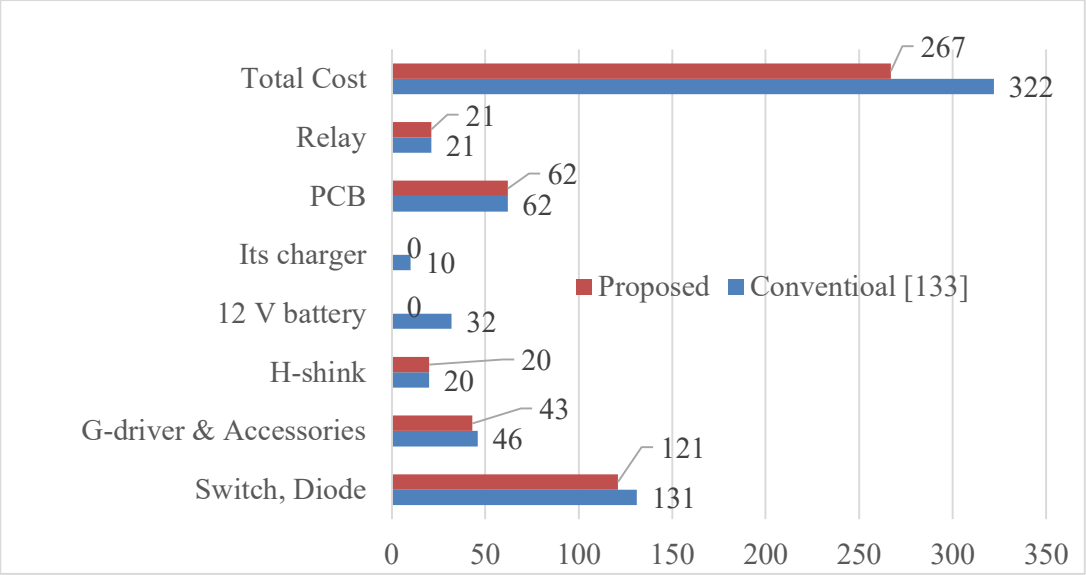

Fig.5. 10 Bar chart of the cost comparative analysis with similar prior work.

5.4.3 Component utilization factor

The component utilization factor (CUF) represents the ratio of the number of components used in a specific mode to the total number of components available in the package, as illustrated in (6)[134]. The utilization factor (CUF) for the G2V, V2G, and MM operation, with similar prior work, and the proposed converter, is given in Table 5. 3. The component utilization factor (CUF) of the proposed converter shows improvement over conventional converters across various operating modes.

$$CUF = \frac{Number\ of\ component\ utialzed}{Number\ of\ component\ present\ in\ package} \tag{6}$$

Table 5. 3 Comparison of CUF in their respective modes

S.N	G2V	V2G	MM
[67]	1	0.75	--
[133]	1	1	0.5
[135]	1	--	0.4
[43]	0.8	--	0.6
P.C	1	1	0.81

Table 5. 4 Available rated voltage in their respective mode of operation

Mode of operation	Input supply	Output available voltages (Volt)		
Charging	120 V (rms), 50 Hz	48 V	72	12
V2V	48 V	48 V	72	12
Motoring	48 V	Variable DC	72	12
V2H	48 V	120 (rms)	72	12
V2G	48 V	120 (rms), 50 Hz	72	12

Table 5. 5 Specification of components used in the proposed converter

Elements	Quantity	Rating
L_{so}	1	2mH
$C_{dc\text{-}link}$	6	470 µF
Transformer	1	740 µH (Lm), 35 µH (Lr), 4:1
Switches	11	650 V, 31 A
Additional Switches	3	450 V, 60 A
Battery	1	48 V, 36 Ah
L_A, L_B	1	1mH, 640 µH
C_{bat}, C_{01}, C_{02}	1	470 µF, 470 µF, 100 µF
Micro-controller	1	TMDSCNCD28335

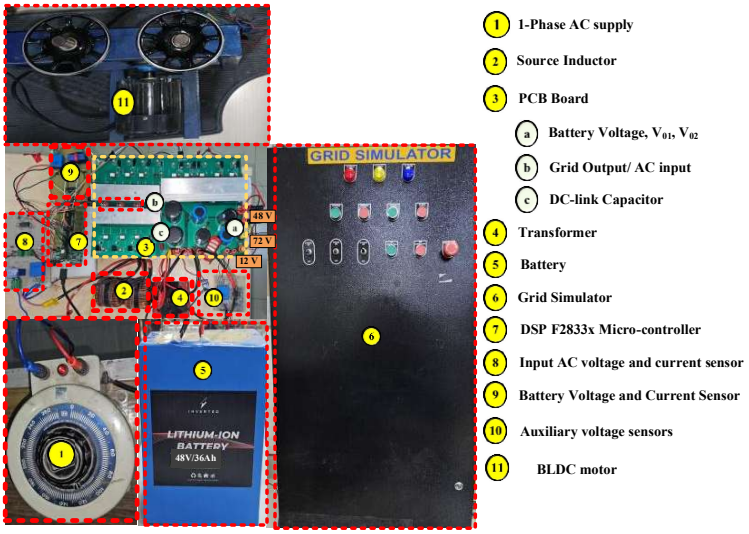

Fig.5. 11 Experimental setup of the proposed converter.

5.5 Experimental validation

The experimental results validate the concepts of the proposed converter in each operating mode. A pictorial representation of the proposed converter is shown in Fig.5. 11. The operating voltage levels during each mode are listed in Table 5. 4 and the ratings of the operating elements are presented in Table 5. 5. The sequence of the results is as follows: G2V operation, V2G operation, motoring mode operation, and vehicle-to-vehicle charging operation.

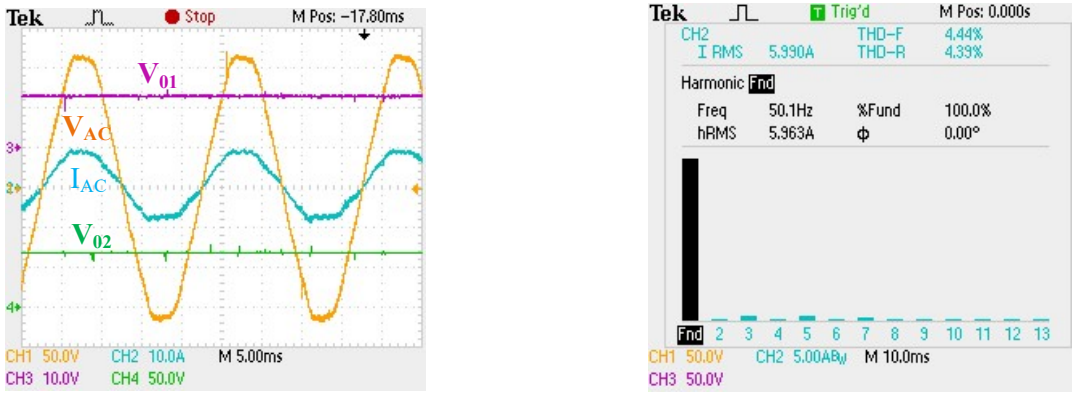

(a) (b)

Fig.5. 12 G2V operation of the proposed power processor, (a) PFC with the auxiliary power supply, and (b) THD spectrum of the source current.

5.5.1 G2V charging operation of the proposed converter

5.5.1.1 PFC operation with the auxiliary power supply

The industry standard IEC61000-3-2 states that the power factor should be greater than 0.98 during single-phase charging. The proposed converter maintains 0.99 PF at the source of a 120V, 50 Hz power supply. During charging, the proposed converter maintains auxiliary voltages of V_{01} (72 V) and V_{02} (12 V) to support the power needs of the EV cabin, as shown in Fig.5. 12(a). The IEEE 519-2014 states that THD should be less than 5 %. In the proposed converter, 4.44 % of the THD-F is maintained, as shown in Fig.5. 12(b).

5.5.1.2 PFC operation and the voltage regulation during load dynamics

The proposed converter sustains the unity power factor during the step change in resistive load, and its response is illustrated in Fig. 11(a). Furthermore, the proposed converter maintains stable voltage regulation during G2V charging, as depicted in Fig. 11(b), where V_{bat} and I_{bat} denote the battery voltage and current, while V_{01} and V_{02} represent the auxiliary supply voltages

of 72 V and 12 V, respectively.

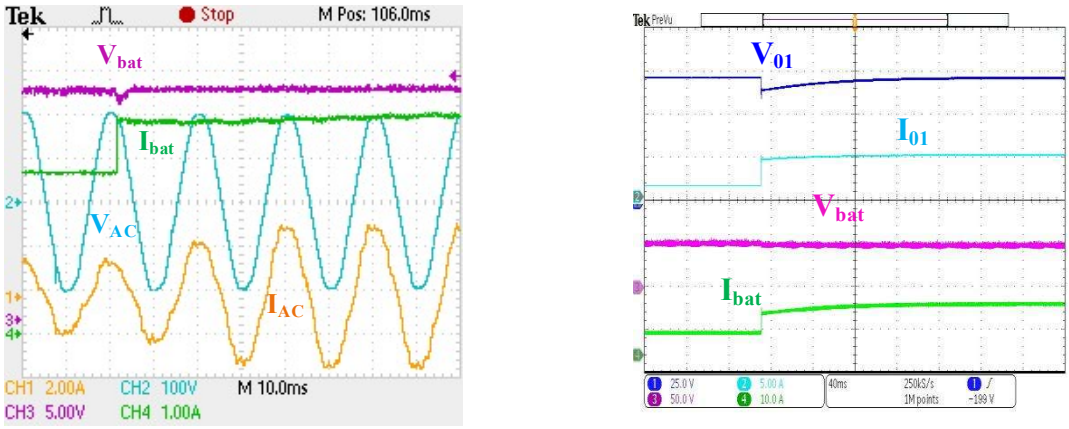

(a) (b)

Fig.5. 13 Load dynamics in G2V operation, (a) during PFC operation, and (b) stable voltage regulation during load dynamics in auxiliaries.

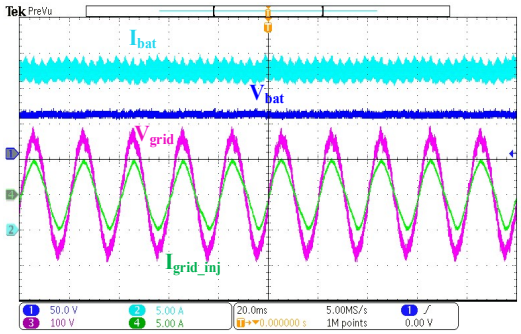

Fig.5. 14 V2G power supply by the proposed converter.

5.5.2 V2G power supply

3.5 A of current is injected into a 120 V, 50 Hz grid bus from the 48 V battery. The V2G operation, along with the battery voltage and current, is shown in Fig.5. 14. One of the key factors in grid-connected systems is phase synchronization between the grid voltage and current, which is achieved in the proposed converter.

5.5.3 Motoring mode operation

5.5.3.1 Torque analysis of the proposed converter during motoring mode

In an electric motor, the load torque is directly proportional to the current. Fig. 13(a) illustrates the motor line current (i_a, i_b, and i_c) with the battery voltage, representing the load torque. The current through the upper and lower switches of the proposed converter in phase-

A, along with their switching behaviour, is depicted in Fig. 13(b) as I_A, I'_A, and V_{A_GS}, respectively. The commutation current ripple associated with the lower switch current (I'_A) is significantly reduced. Similarly, the commutation current ripple in the lower switch currents of proposed converter phases B and C (I'_B and I'_C) is also effectively minimized.

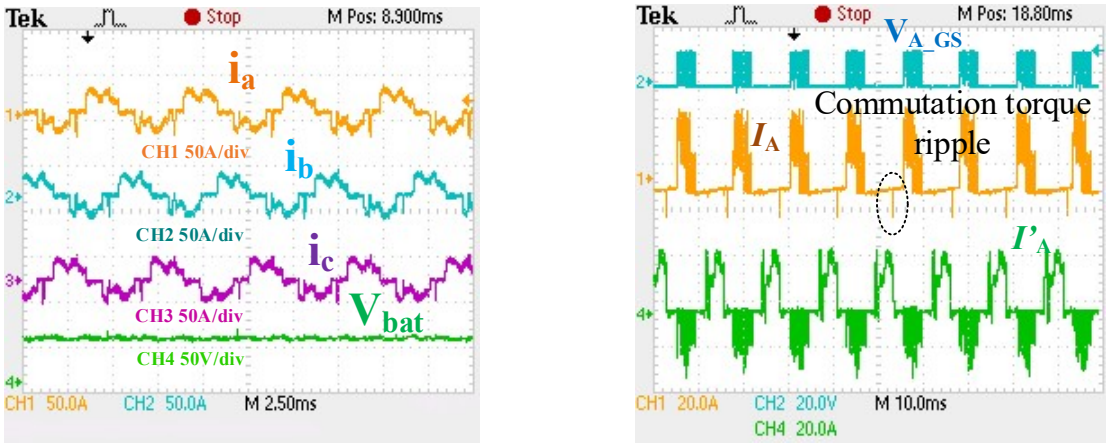

(a) (b)

Fig.5. 15(a) converter line current ia, ib, and ic with battery voltage during motoring operation, and (b) converter switch current of one-leg with drain to source voltage on switch S1, while driven with High-PWM Low-ON switching scheme.

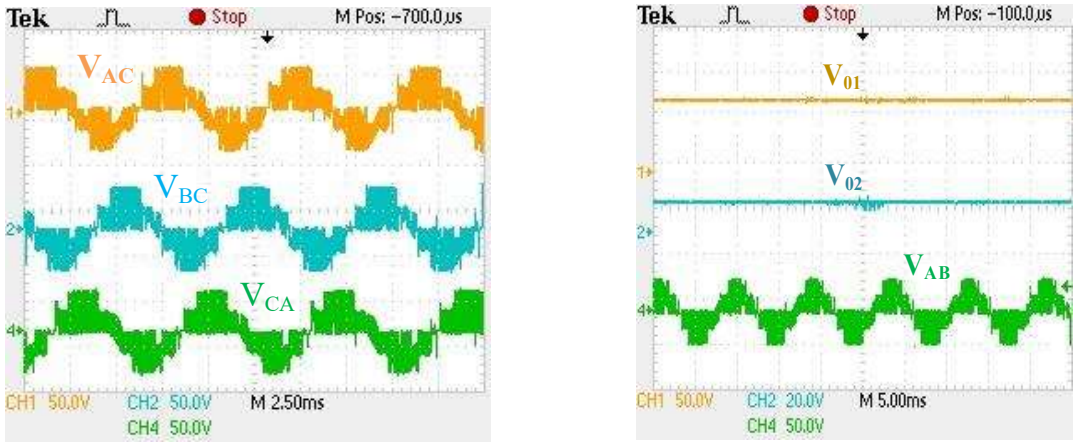

(a) (b)

Fig.5. 16 In motoring mode operation, (a) line voltages and (b) auxiliary voltages with the line voltage of the proposed converter.

5.5.3.2 Converter voltage during motoring operation

During the motoring operation, the line voltages (V_{AB}, V_{BC}, and V_{CA}) of the proposed converter are shown in Fig.5. 16(a), which are 120^0 phase-shifted from each other. The auxiliary supply voltages V_{01}(72 V) and V_{02} (12 V) with the line voltage V_{AB} are shown in Fig.5. 16(b).

5.5.3.3 Dynamic operation during motoring mode

During motoring mode, a resistive load dynamic is applied in the high-power auxiliary, and the stable voltage regulation is shown in Fig.5. 17(a). Where V_{AB} represents the line voltage, and V_{01}, V_{02}, and I_{01} represent the auxiliary voltages and the high-power auxiliary load current. Further, the resistive load dynamic is applied at the low-power auxiliary, and stable voltage regulation is shown in Fig.5. 17(b).

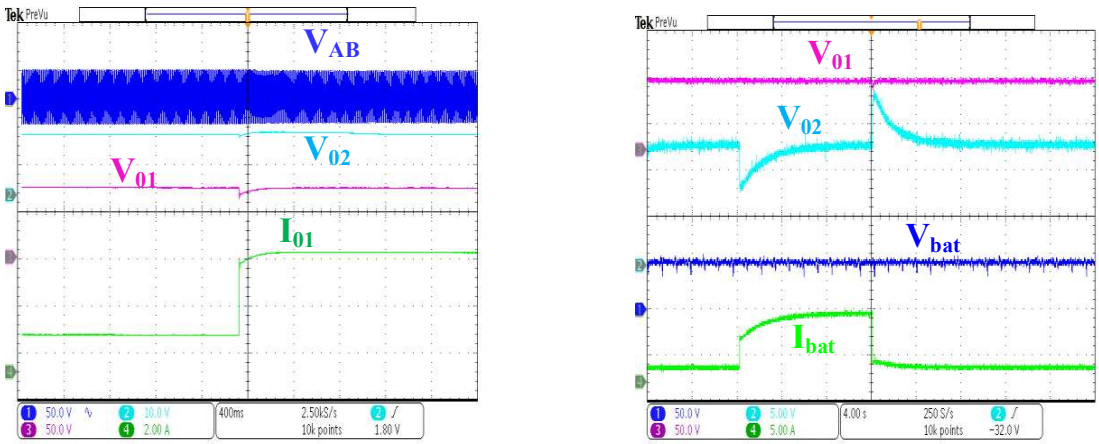

(a) (b)

Fig.5. 17 Load dynamics during motoring operation, (a) load dynamic is applied in the high-power auxiliaries, and (b) load dynamic is applied in the low-power auxiliaries.

5.5.4 V2V charging operation of the proposed converter

5.5.4.1 Converter switching operation during V2V charging

For V2V charging, the proposed power converter from both vehicles is directly connected for the energy exchange. The energy supplier vehicle drains to source switching voltages ($V_{A\text{-}DS}$ and $V_{B\text{-}DS}$) of switch S_A and S_B, along with the current profile of the inductors L_A and L_B during V2V charging, is shown in Fig.5. 18(a). In a similar way, the operation of the energy acceptor vehicle is shown in Fig.5. 18(b). Where I_{LA} shows the current profile of the inductor L_A of the energy acceptor vehicle, along with the drain-to-source voltage of the switch S_C. Further, $V_{bat\text{-}1}$ and $V_{bat\text{-}2}$ show the battery voltages of the energy supplier and the acceptor vehicle.

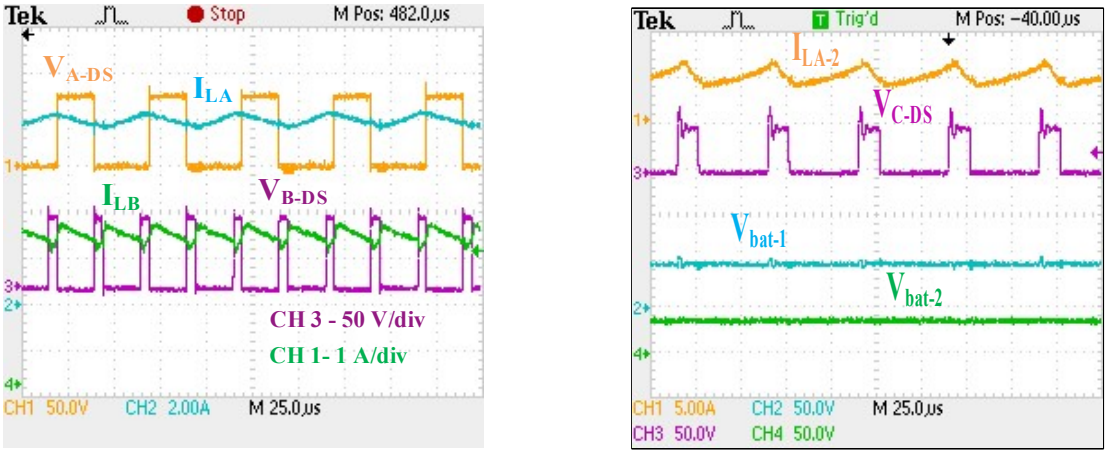

(a) (b)

Fig.5. 18 (a) $V_{A\text{-}DS}$ and $V_{B\text{-}DS}$ are the drain-to-source voltages of the switch S_A and S_B with the inductor L_A and L_B current profile of the energy supplier vehicle, and (b) energy supplier and acceptor vehicles' battery voltages with inductor current profile and drain-to-source voltage ($V_{C\text{-}DS}$) of the switch S_C of the energy acceptor vehicle.

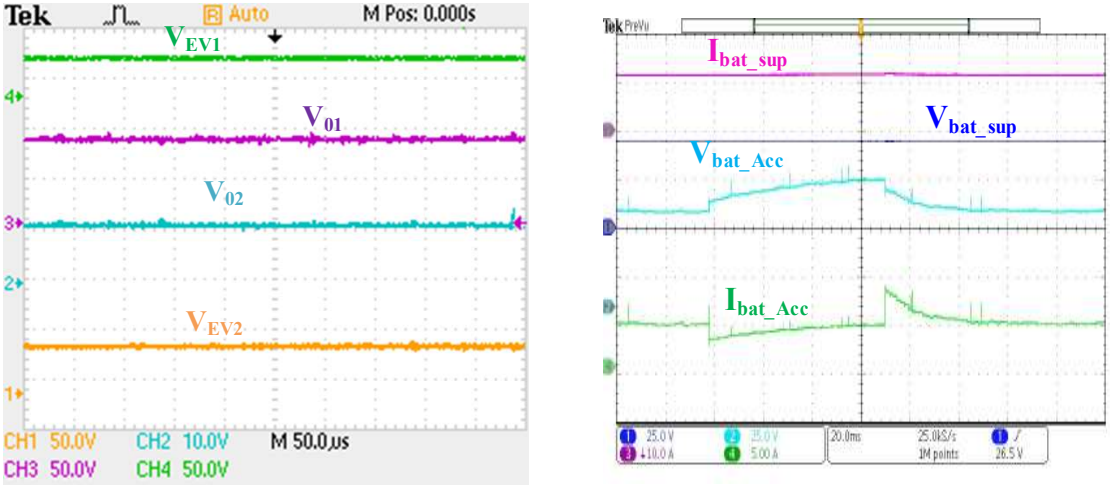

(a) (b)

Fig.5. 19 V2V charging operation, (a) available voltages, and (b) constant current charging of the acceptor vehicle remains sustained while a resistive load transient is applied to the acceptor vehicle battery terminal.

5.5.4.2 Available voltages and the load dynamics during V2V charging

The auxiliary power supply of the energy supplier vehicle remains active during V2V charging. The high-power auxiliary supply source, 72 V, is used to form the connection between the energy suppliers and the acceptor vehicle. The available voltages during V2V charging are shown in Fig.5. 19(a), where V_{EV1}, V_{01}, and V_{02} are the supplier vehicle battery voltage and auxiliary power supply, and V_{EV2} represents the acceptor vehicle battery voltage. The rate of

charge of the acceptor vehicle is controlled by the constant-current charging value of the acceptor vehicle. A resistive load is used to validate the CC charging of the acceptor vehicle during the load transient, as shown in Fig.5. 19(b).

5.6 Conclusion

In this chapter, a reversible multifunction multimode on-board power processor with inherent V2G operation is proposed. It performs grid-to-vehicle (G2V) charging, vehicle-to-grid (V2G) power supply, motoring operation (MM), vehicle-to-vehicle charging, and auxiliary power supply for the EV cabin. All these functions are implemented with the 14 switches, which are smaller but have more functionalities compared to similar prior works. During G2V operation, it charges the 48V battery from the 120V, 50Hz power supply and generates two more outputs of 12V and 72V to supply the low-power and high-power auxiliaries of the EV cabin. In V2G operation, the 3.5 A current is injected into a 120 V, 50 Hz AC grid system. In motoring mode, it drives the BLDC motor with a High-PWM Low-ON switching scheme and generates regulated output voltages (12 V and 72 V) from the 48 V battery. The 12 V regulated output eliminates the demand for an additional low-voltage battery (12 V), and its charger and 72 V output reduce the current demand for the high-power auxiliaries in low-power EVs. To express the novelty, comparative analysis, cost analysis, and component utilization factor have been expressed with similar prior works. To justify the proposed idea, the multifunction operation, control algorithm, and experimental results with load dynamics are presented. A laboratory-scale prototype is tested at 780 W in G2V changing operation, 1 kW during V2G operation, 1 kW in motoring operation, and 480 W in V2V charging.

The work carried out in this chapter has some limitations: 1) Three changeover switches are still used for the selection of the operating mode. 2) it supports only the low-power EV applications, where it can drive only a 48 V-rated motor like BLDC.

The next chapter introduces an improved architecture by eliminating the changeover switches and replacing them with a newly designed, more reliable circuit. Thereby significantly improving the overall efficiency of the EV power processor. This new configuration not only enhances the durability of the system but also supports high-power EV motors like induction motors (IM) and permanent magnet synchronous motor (PMSM).